MIE 418 Final Project

NACA 1408

Young Kwon

997742750

April 8th, 2014

Mechanical & Industrial Engineering
UNIVERSITY OF TORONTO

1. INTRODUCTION

The following report shows the simulation and numerical analysis of turbulent flow over an airfoil using the *Spalart-Allmaras equation*. The airfoil in this instance was NACA-1408 (an asymmetrical model). Analyses were performed for various angles of attack (α = -5, 0, 5, 10). Both a coarse and fine mesh were used to confirm that the numerical method, geometry and mesh were accurate.

Assumptions Made

Re = **100,000** Density (ρ) = **1.225** kg/m^3 Dynamic viscosity (μ) = **1.7894 x 10^{-5}** Pa·s

Chord length (L) = **1** m $P_{inlet} = P_{outlet} =$ **0** Pa

2. GEOMETRY AND MESH

2.1 Sizing and Biasing of Mesh

The geometry of the mesh used was a C-Mesh to simulate the air flow over the airfoil. The distance (12m) of the C-Mesh from the airfoil was kept at about 12 times the chord of the airfoil which was (1m). As mentioned before, a coarse and a fine mesh were used to evaluate the legitimacy of the method used. For the coarse mesh, the straight edges of the mesh were given 50 divisions and a bias of 350. The C section of the mesh and the airfoil were given 100 divisions and no bias. For the fine mesh, 100 divisions were given to the straight edges of the mesh and a bias of 350. For the C section of the mesh and the airfoil, 200 divisions were given.

Figure 1: Coarse (*left*) and Fine (*right*) Mesh

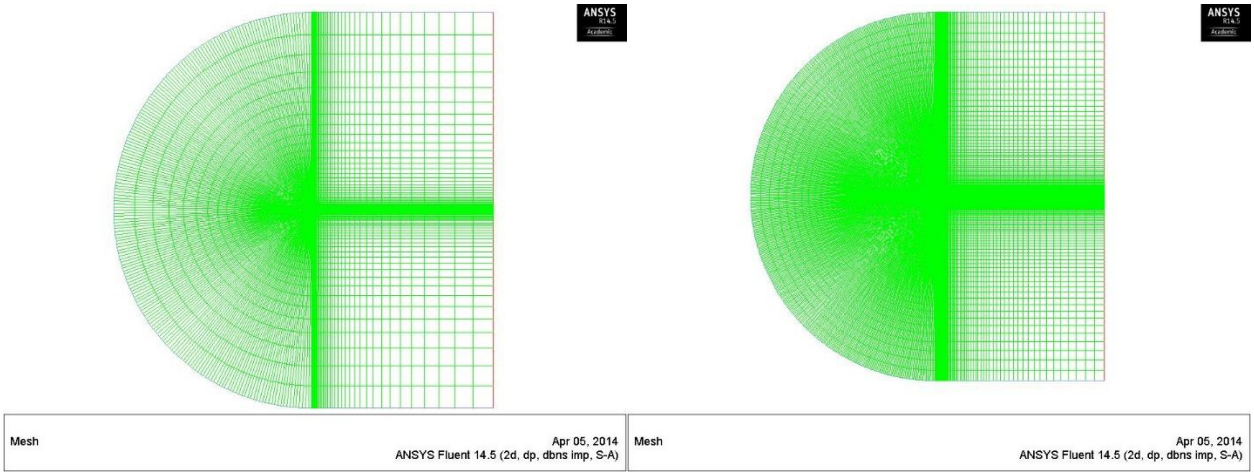

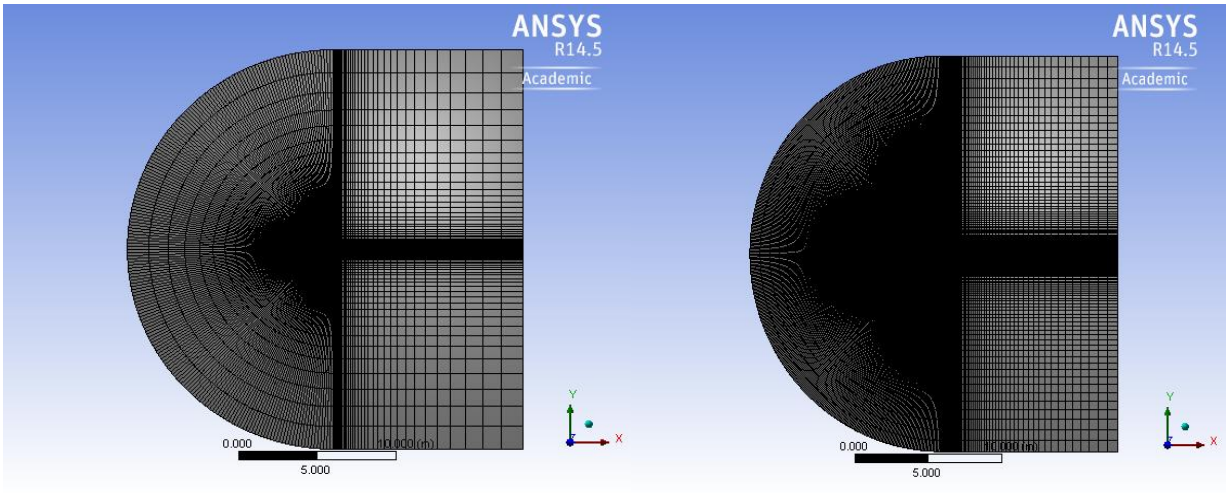

Figure 2: Edge Sizing for Coarse (*left*) and Fine (*right*) Meshes

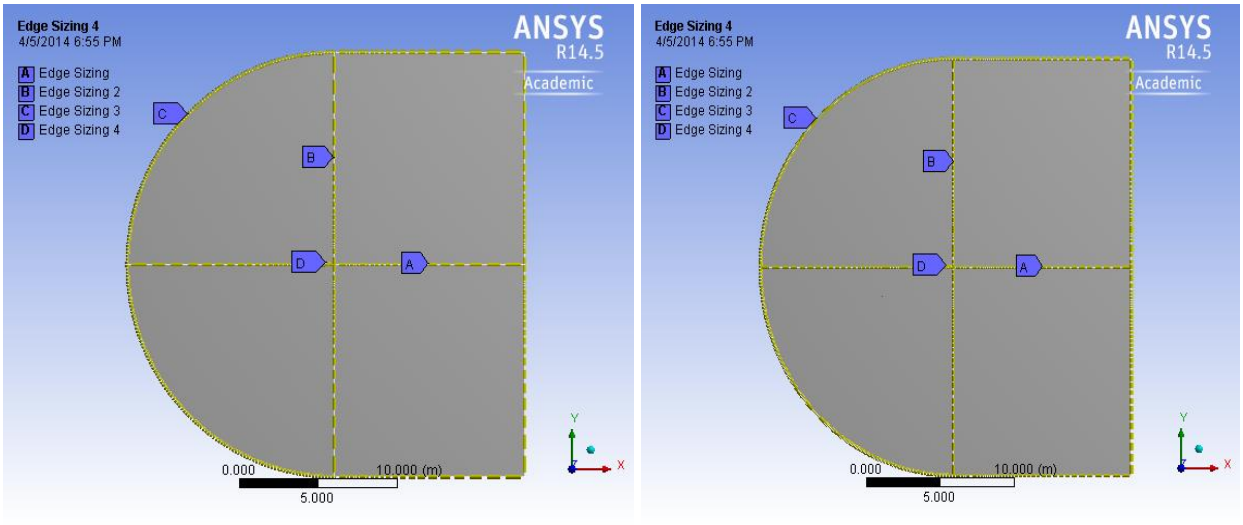

2.2 Refinement Strategy

The mesh was refined closer to the actual airfoil as shown in the figure below. This was done to simulate the boundary layer effects on the airflow over the airfoil. Obviously the closer the air is to the airfoil, the slower the air will flow because of the wall of the airfoil and so more nodes were added to simulate this effect. On the other hand, the further the flow is from the airfoil, the less effect there is from the walls of the airfoil and so they were left untouched.

Figure 3: Refinement of Mesh

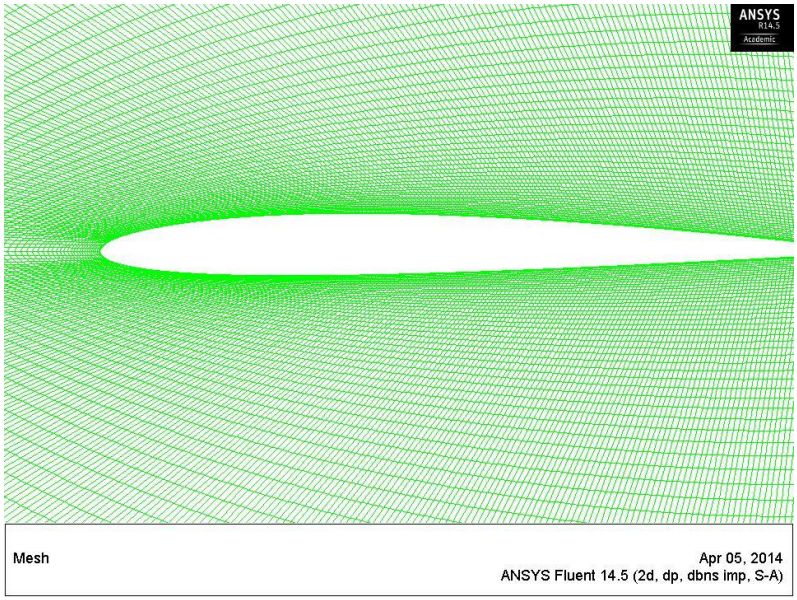

3. VELOCITY ACCORDING TO ANGLE OF ATTACK

Because it is time-consuming to constantly change the geometry of the mesh for each angle of attack, the velocity components in the x and y direction were changed to achieve the same results as having the airfoil angled to the flow of air. The velocity magnitude was calculated from the given Reynolds number:

$$V = \frac{Re\mu}{\rho L} = \frac{(100{,}000)(1.7894 * 10^{-5}\ Pa \cdot s)}{(1.225 kg/m^3)(1\ m)} = \mathbf{1.4607}\ m/s$$

$$V_x = V \cos\alpha = (\frac{1.4607m}{s})(\cos(-5°)) = \mathbf{1.4551}\ m/s$$

$$V_y = V \sin\alpha = \left(\frac{1.4607m}{s}\right)(\sin(-5°)) = -\mathbf{0.1273}\ m/s$$

This magnitude was constant for each simulation of the airfoil no matter what the angle of attack; however, the x and y components changed accordingly as shown below:

Table 1: X and Y Velocity Magnitudes of the Airflow

Angle of attack α (°)	X-Component (m/s)	Y-Component (m/s)
-5	1.4551	-0.1273
0	1.4607	0
5	1.4551	0.1273
10	1.4385	0.2536

4. CONVERGENCE PARAMETERS

4.1 Residuals

In order to confirm the convergence of the values, the residual values of the x-velocity, y-velocity, continuity and nut had to be at least 10^{-6}. This was confirmed as shown by the graph below. For each angle of attack and mesh type, the number of iterations required to converge changed.

Figure 3: Residual Values of Simulation

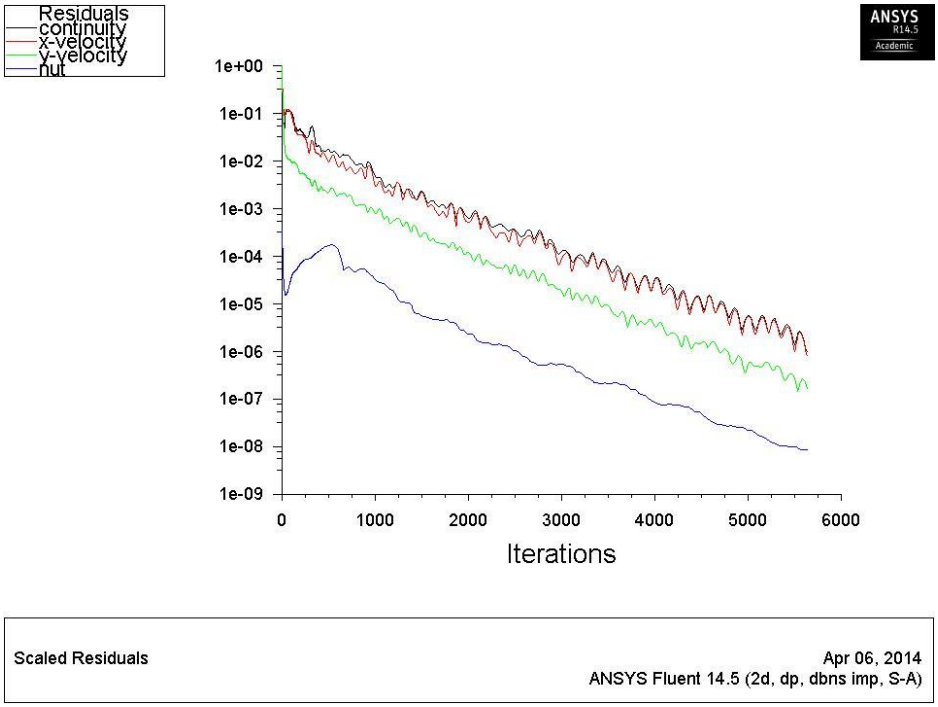

4.2 Convergence of C_L and C_D

Another important criterion to fulfill was to confirm that lift and drag coefficients converged to a stable value and did not change over the number of iterations. The figure below shows the convergence of both coefficients over the number of iterations. It only shows the convergence of one angle of attack, but the values for the other angles have converged but required more iterations.

Figure 4: Drag Coefficient Convergence of α = -5

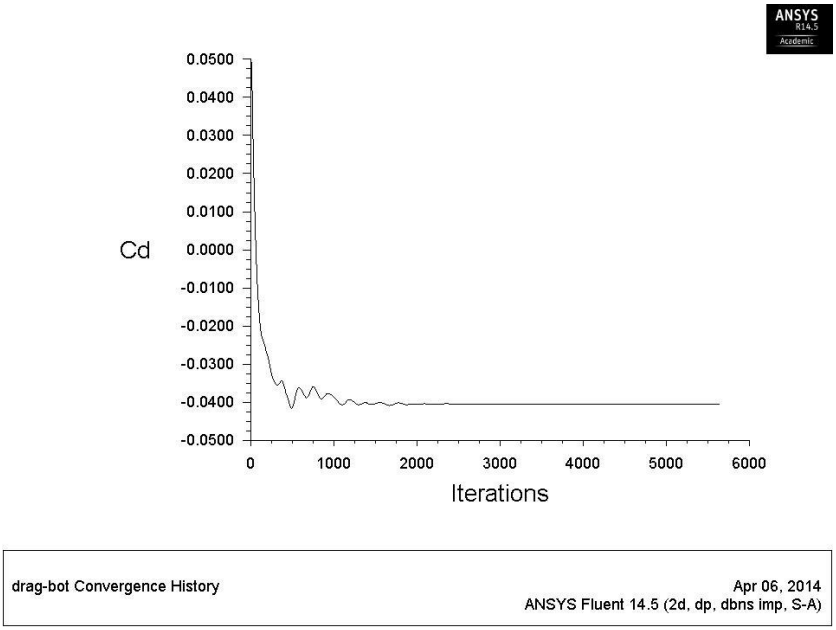

Figure 5: Lift Coefficient Convergence of α = -5

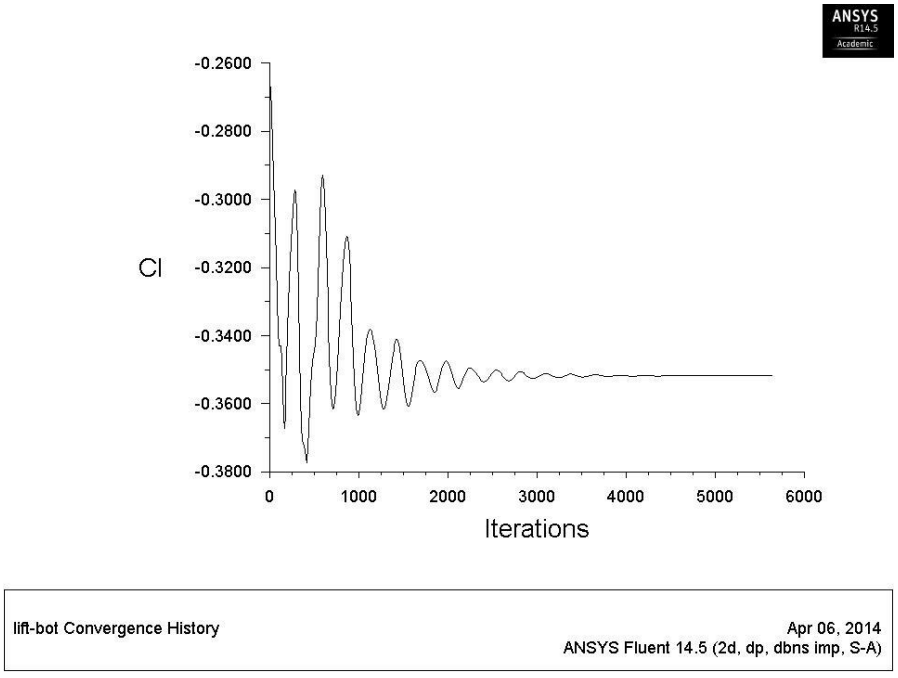

4.3 Wall Yplus

The following plot shows the Y^+ values for the airfoil wall. The values are mostly on the order of 1 which legitimizes the accuracy of the simulation.

Figure 6: Wall Y+ Values for Both the Top and Bottom of the Airfoil

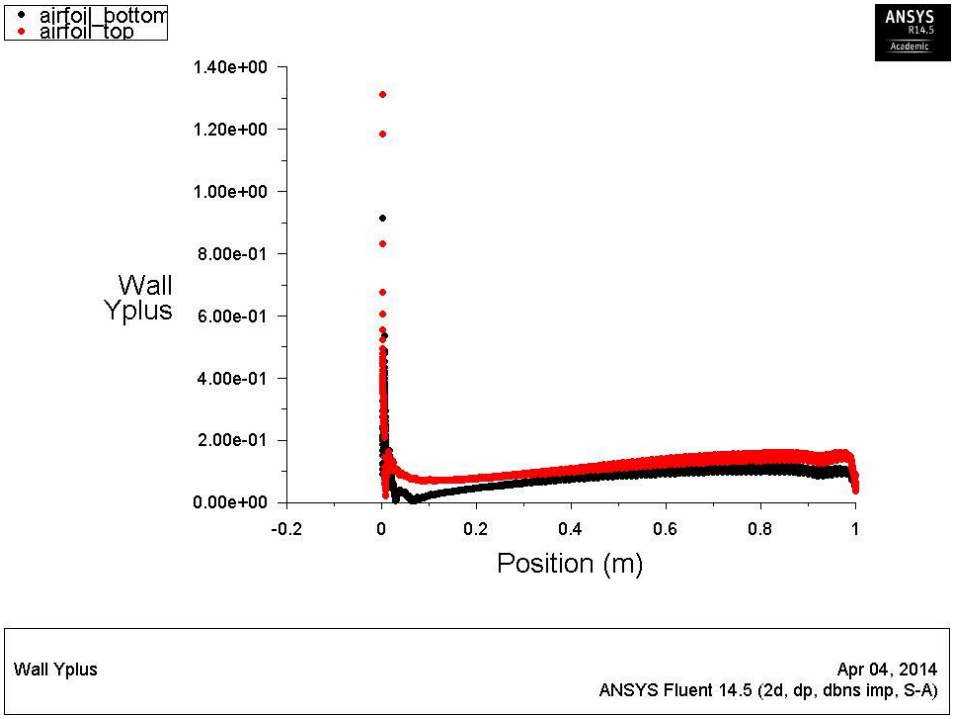

5. COMPARISON OF DRAG AND LIFT COEFFICIENTS

5.1 Comparison of Airfoil-Tools and Simulation Values

The following tabulated data and graphs show the difference between the drag and lift coefficients generated in the simulation and the values given by Airfoil-Tools. Values were chosen for Ncrit = 9 (most typical turbulence) and Re = 100,000.

Table 2: Drag Coefficients (*Coarse Mesh*)

Angle of attack α (°)	**ANSYS (FLUENT)**	**Airfoil-Tools**
-5	0.02676	0.02359
0	0.01753	0.01192
5	0.02338	0.01820
10	0.1115	0.11037

Figure 7: Graph Comparison of Drag Coefficients

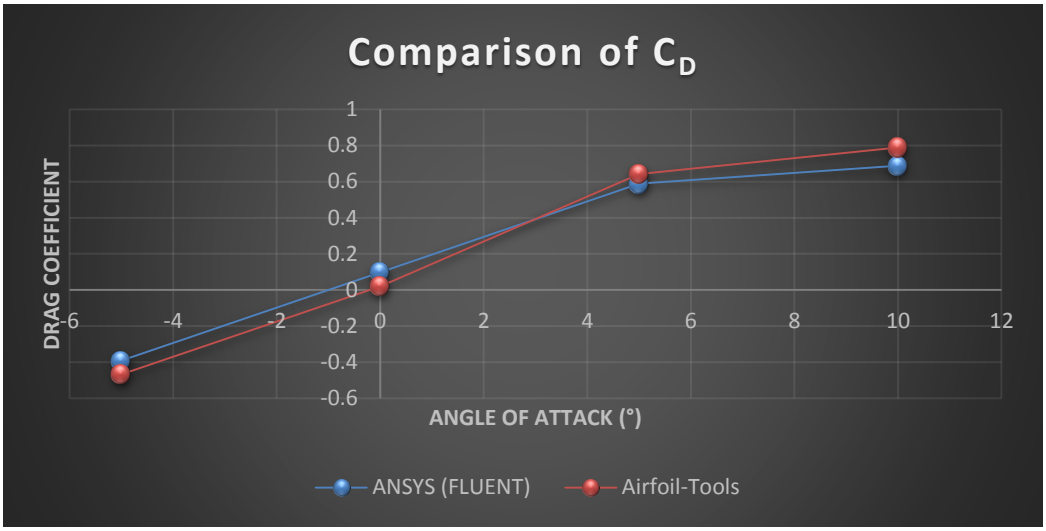

Table 3: Lift Coefficients (*Coarse Mesh*)

Angle of attack α (°)	**ANSYS (FLUENT)**	**Airfoil-Tools**
-5	-0.3902	-0.4678
0	0.09838	0.0198
5	0.5896	0.6420
10	0.6878	0.7899

Figure 8: Graph Comparison of Lift Coefficients

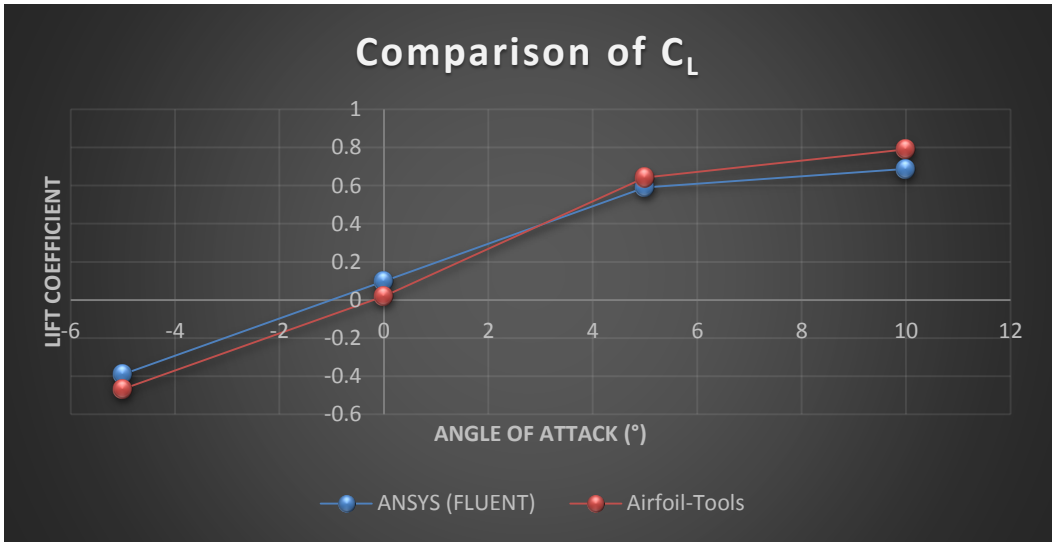

As can be seen by the tabulated data and graphs, the values of the simulation and Airfoil-Tools were fairly close which legitimizes the accuracy of the simulation.

5.2 Comparison of Coarse and Fine Meshes

For the comparison of the coarse and fine meshes, it can be observed that for some of the angles of attack the difference is less than 5% while others have much larger differences. This weakens the division strategy between the fine and coarse meshes, and it should be noted that more proper divisions must be made for future applications.

Table 4: Comparison of Coarse and Fine Mesh (*Drag Coefficient*)

Angle of attack α (°)	**Coarse**	**Fine**	**Difference (%)**
-5	0.02676	0.02173	18.79671
0	0.01753	0.01615	7.872219
5	0.02338	0.02164	7.442258
10	0.1115	0.1057	5.201794

Figure 9: Graph Comparison of Drag Coefficients (*Coarse and Fine*)

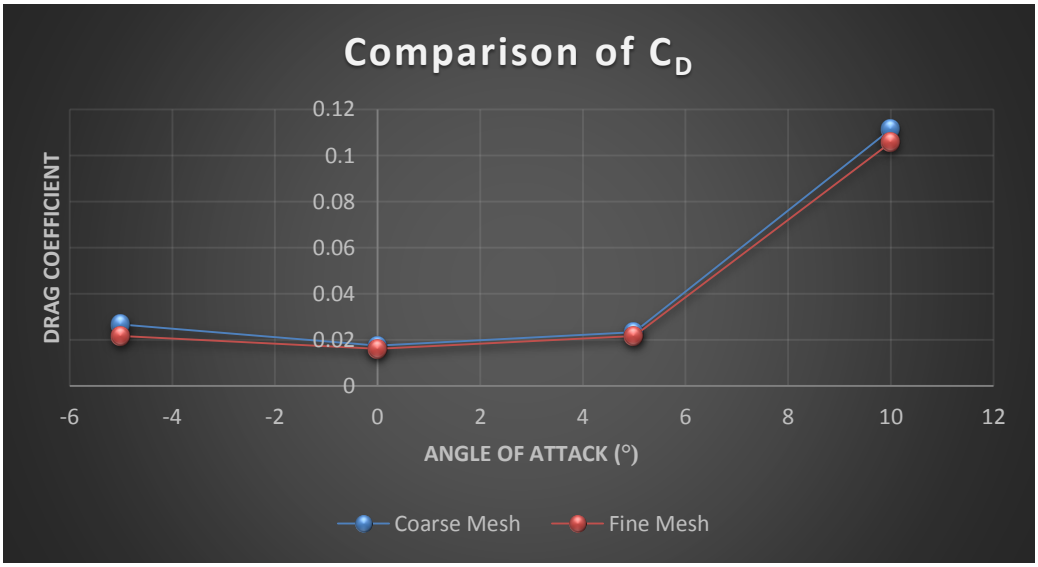

Table 5: Comparison of Coarse and Fine Mesh (*Lift Coefficient*)

Angle of attack α (°)	**Coarse**	**Fine**	**Difference (%)**
-5	-0.3902	-0.4042	3.5879
0	0.09838	0.09905	0.68103
5	0.5896	0.5943	0.79715
10	0.6878	0.8576	24.6874

Figure 10: Graph Comparison of Lift Coefficients (*Coarse and Fine*)

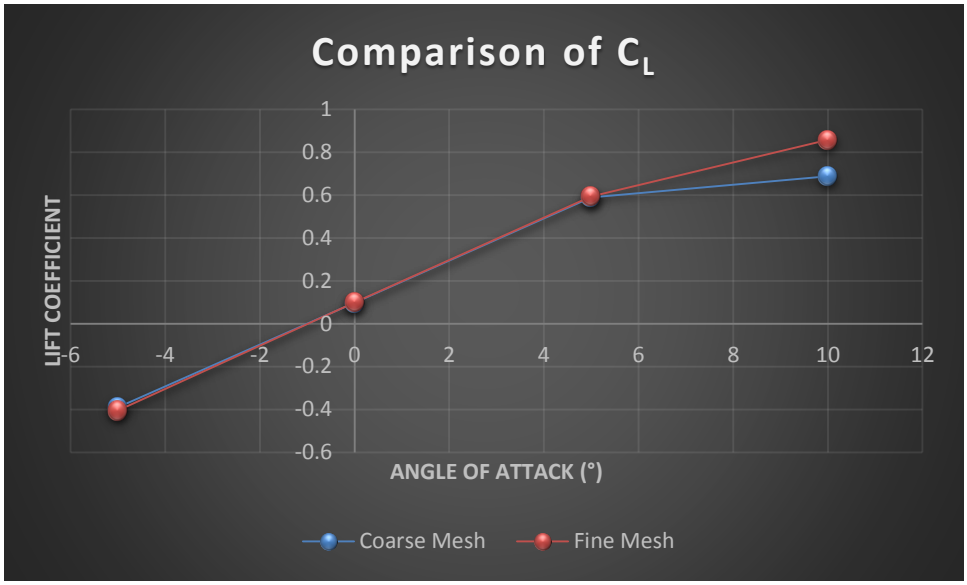

6. PRESSURE AND SKIN COEFFICIENTS

The following figures show the pressure and skin coefficients for each angle of attack for both the top and bottom of the airfoil. Unfortunately, I was unable to plot both quantities on one graph; however, it is easy to make some simple comparisons on how the value of each coefficient changes as the angles change. It is noted that the skin friction coefficient is very small for all cases of angles of attack except $\alpha = 0°$. To us, this makes sense as this is turbulent flow and the viscosity (shear forces) should have minimal to negligible impacts on the airflow.

For $\alpha = -5°$

The pressure coefficient for the top of the airfoil is positive while the pressure coefficient for the bottom is negative. This indicates that there is a pressure gradient going from top to bottom which is equivalent to saying that the overall force is acting in the negative y-direction. Again, this makes sense as the nose of the airfoil is angled downward from the airflow and most of the flow will be hitting the curved section of the top of the airfoil causing an overall downward force. However, this force is very small as the angle is very small.

For $\alpha = 0°$

All of the flow is in the x-direction and so the pressure on both the top and bottom of the airfoil should essentially be the same. However, the geometry of this particular airfoil causes the top of the airfoil to have a slightly higher pressure force acting on it than the bottom. Because of this, the skin friction coefficient actually contributes a significant amount to the drag.

Figure 11: Pressure Coefficient for α = -5°

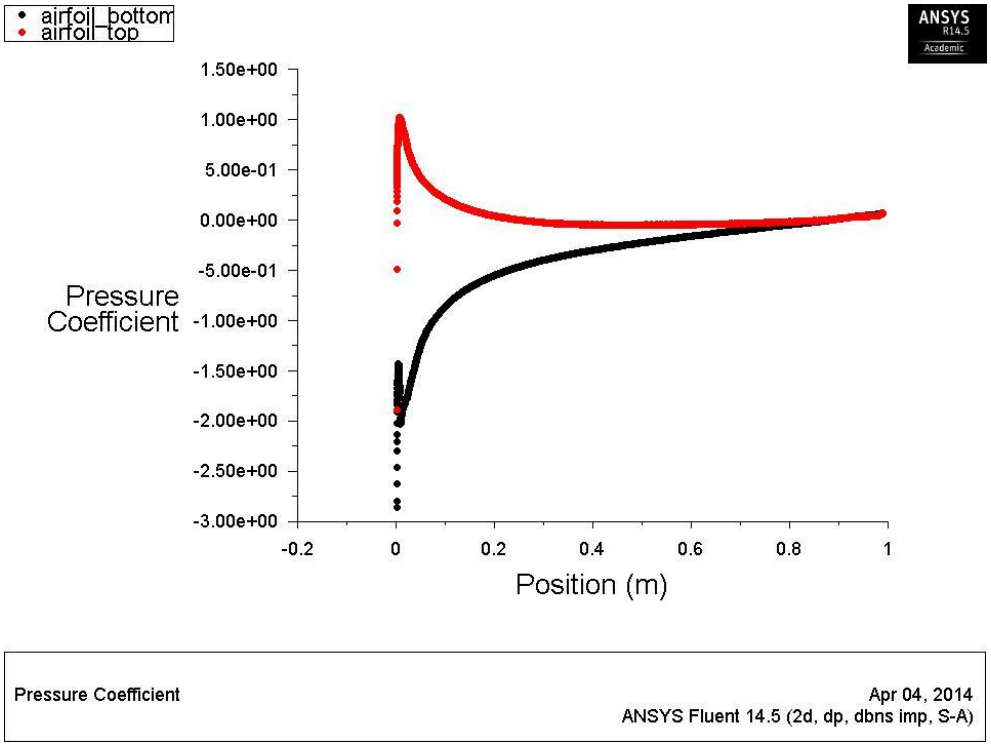

Figure 12: Skin Friction Coefficient for α = -5°

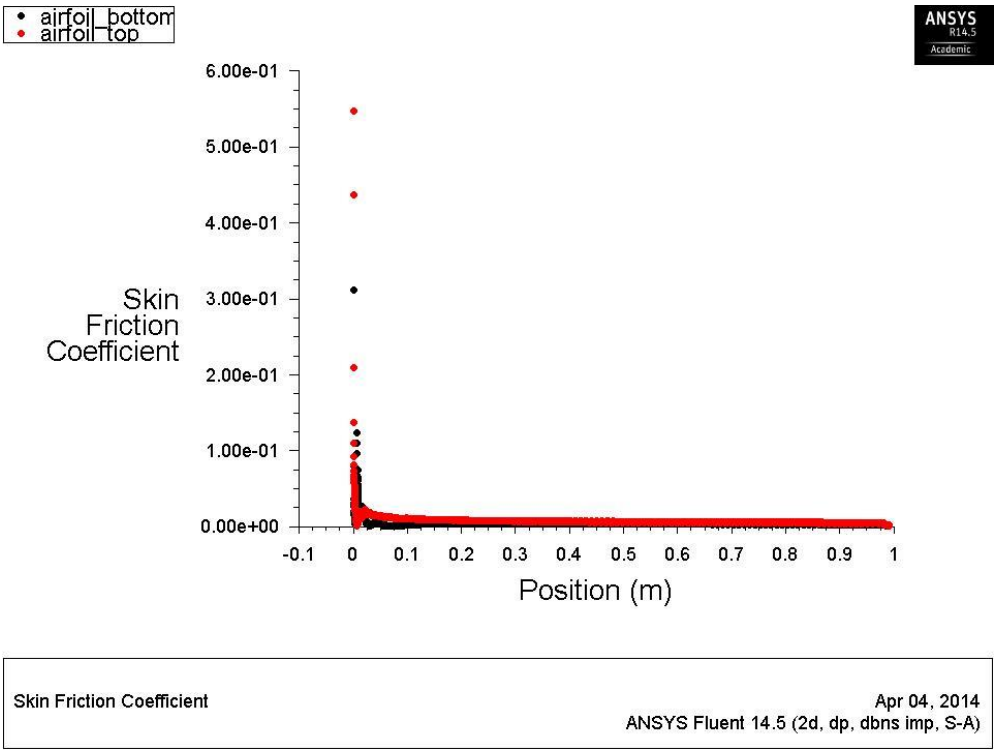

Figure 13: Pressure Coefficient for α = 0°

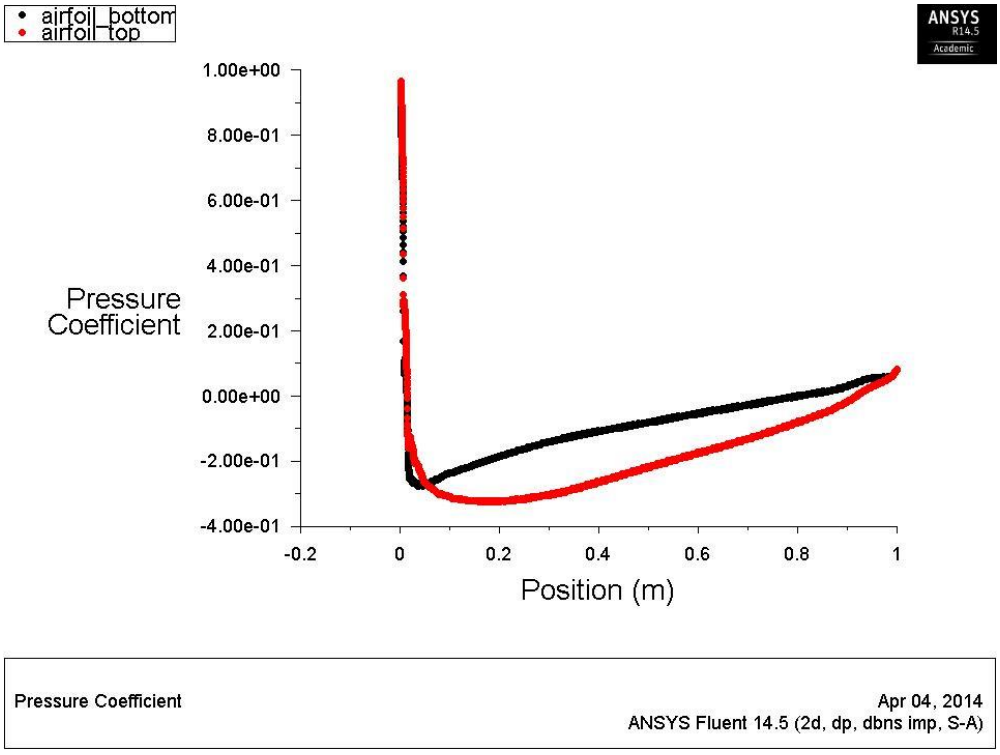

Figure 14: Skin Friction Coefficient for α = 0°

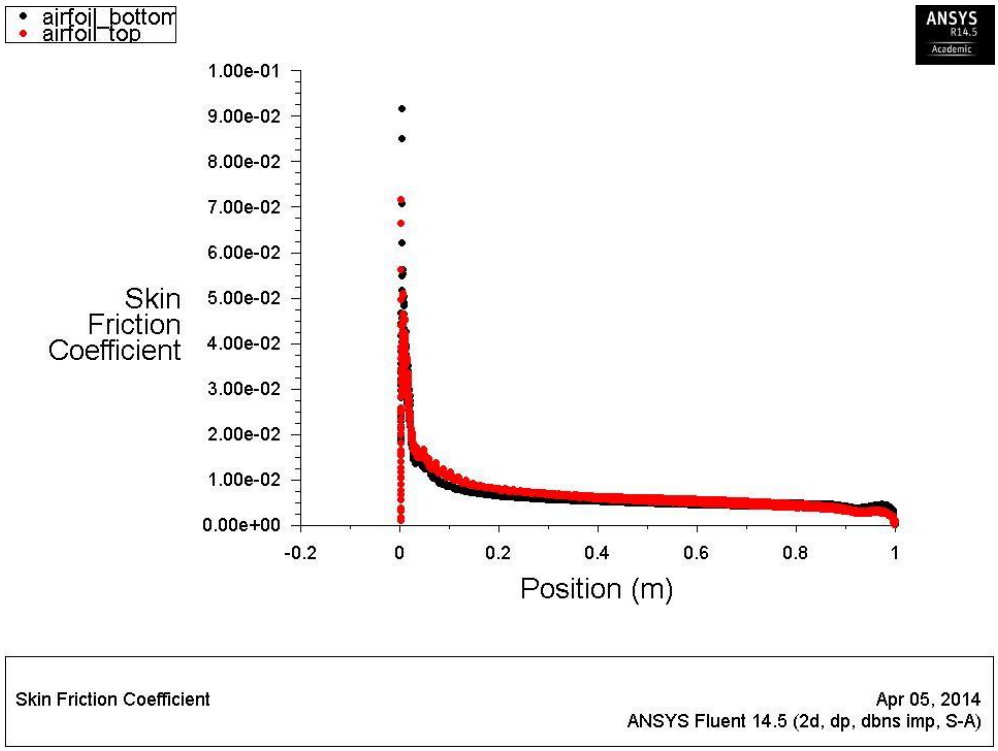

Figure 15: Pressure Coefficient for α = 5°

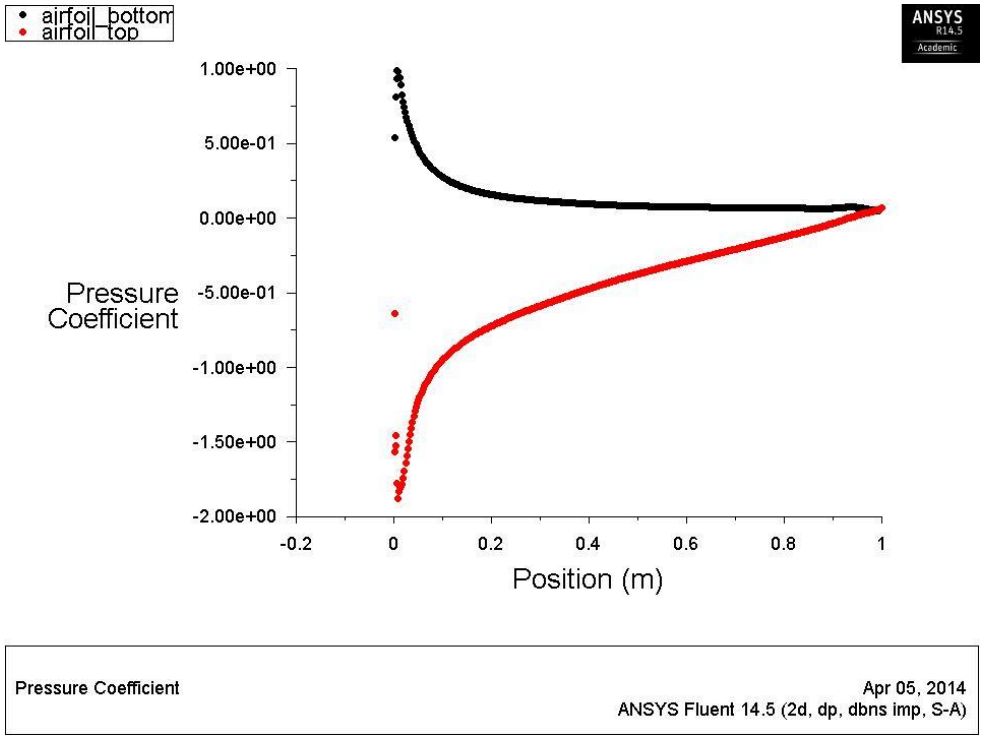

Figure 16: Skin Friction Coefficient for α = 5°

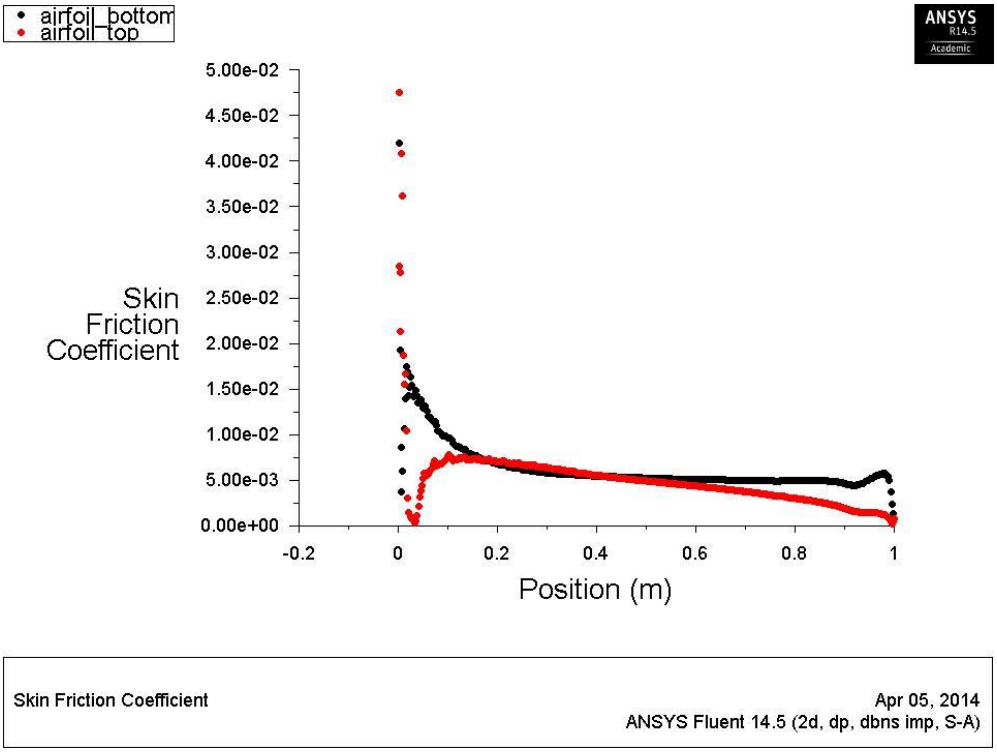

Figure 17: Pressure Coefficient for α = 10°

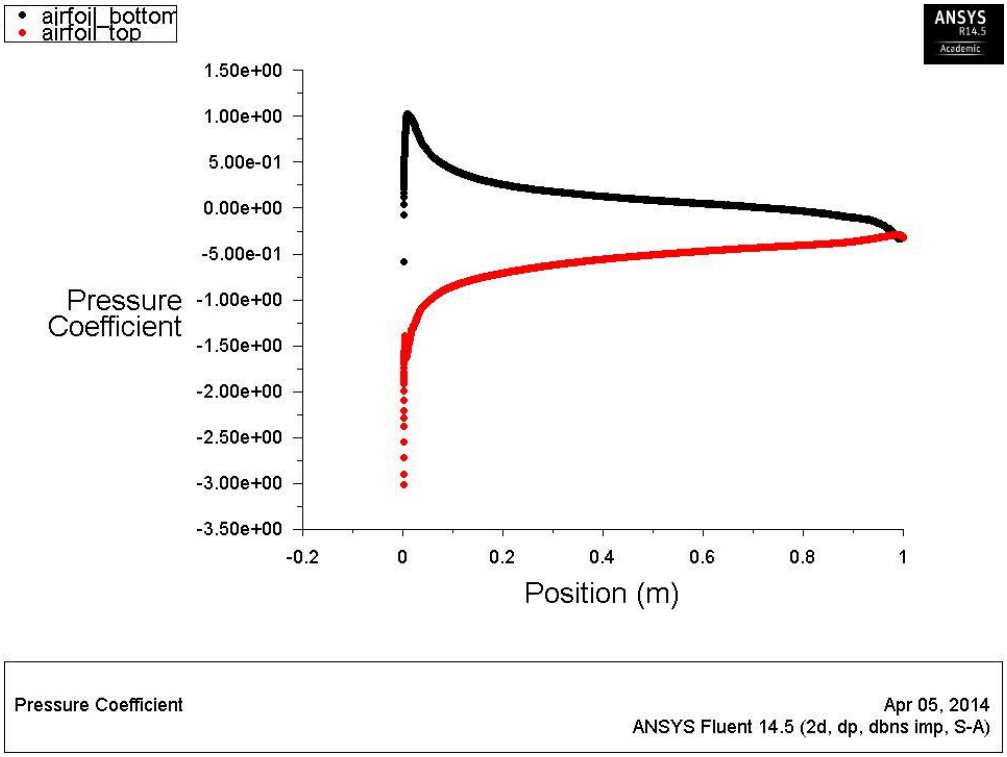

Figure 18: Skin Friction Coefficient for α = 10°

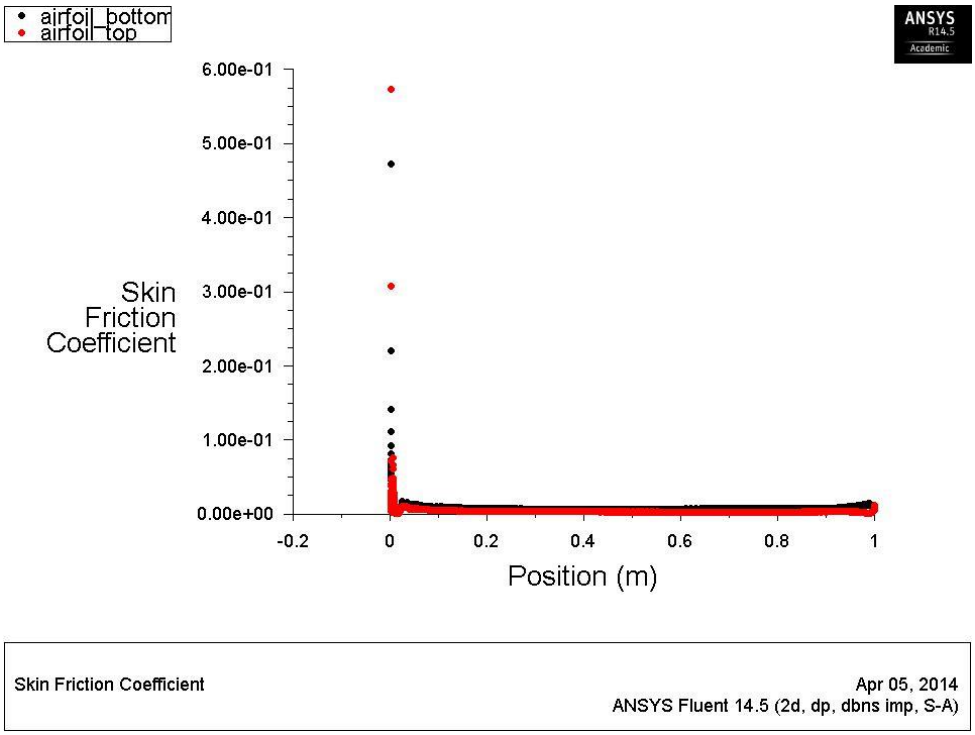

For α = 5°

In this case, the nose of the airfoil is angled slightly towards the positive y-direction and more of the flow will slow down at the bottom of the airfoil. This will cause an increase in pressure as shown in Figure 15. On the other hand the bottom of the airfoil has a negative pressure coefficient which causes an overall pressure force in the positive y-direction.

For α = 10°

This case is similar to the case where α = 5 except it is angled even more in the positive y-direction. Therefore, the values of the pressure coefficients will be higher in magnitude than in the previous case but the directions will be the same.

7. VELOCITY CONTOURS

The following section shows the various velocity contours for each angle of attack. Looking at Figure 19 where the angle is negative, the visual representation is accurate in terms of a fluid mechanics perspective. Since the air has a component of its velocity flowing in the negative y-direction, the flow at the top of the nose of the airfoil is slower than the rest. Additionally the bottom of the 'tail' of the airfoil has a slower velocity due to the fact that very little flow is actually reaching that area.

Figure 19: α = -5°

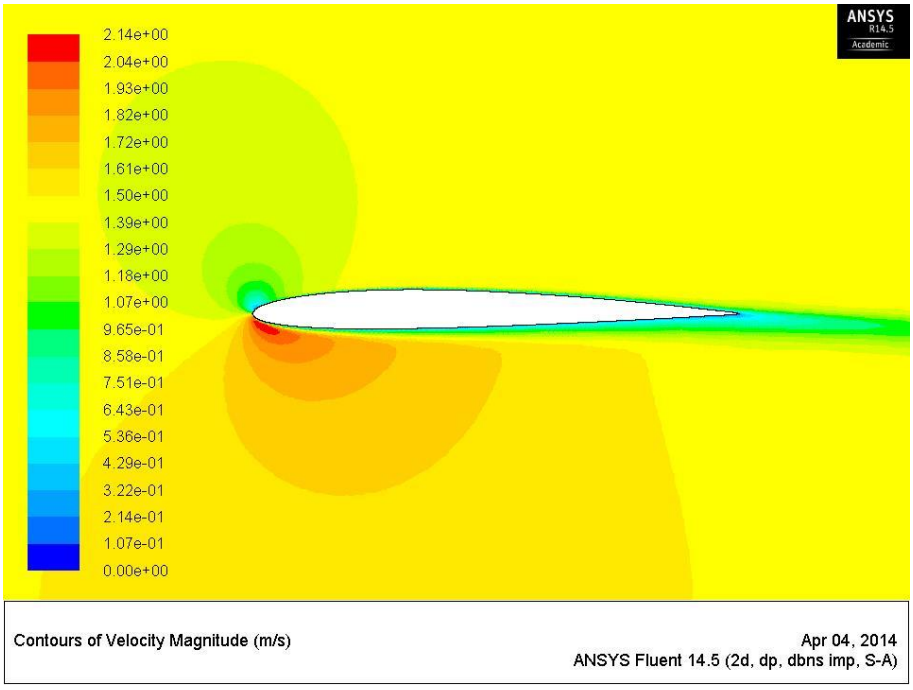

Figure 20: $\alpha = 0°$

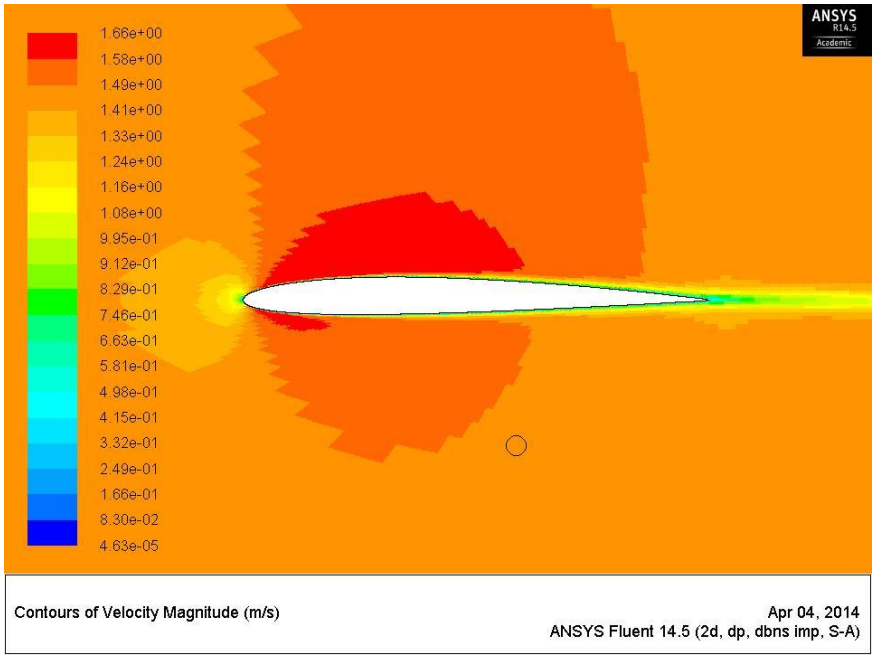

Looking at Figure 20 where all of the velocity is flowing the x-direction, the overall velocity is higher than the previous case. The tip and tail of the airfoil have slower velocities as they are causing stagnation and separation points. Another aspect to note is the difference in velocity magnitudes between the top and bottom of the airfoil. The top has a higher velocity due to the fact that the geometry of the airfoil seems to divert more of the flow to the top half.

Figure 21: Velocity Contour of $\alpha = 5°$

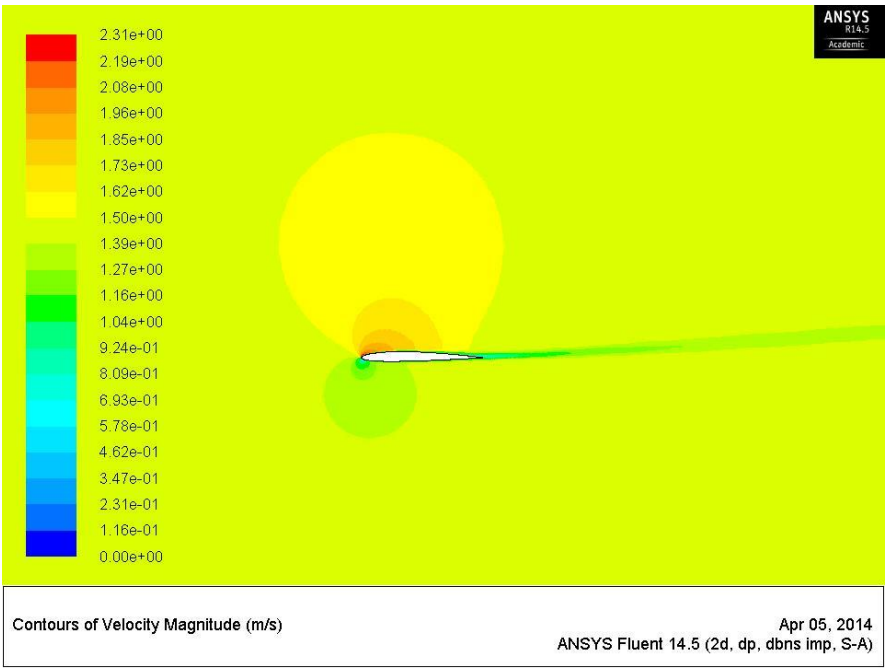

Looking at Figure 21, the overall velocity is much slower than the previous case. The bottom of the tip and the top of the tail of the airfoil have slower velocities as they are stagnation and separation points. The bottom has a slower velocity due to the fact that the angle is causing the flow to hit the bottom of the airfoil and slow down. This confirms the reason why the pressure coefficient increased for the bottom of the airfoil.

Figure 22: Velocity Contour of $\alpha = 10°$

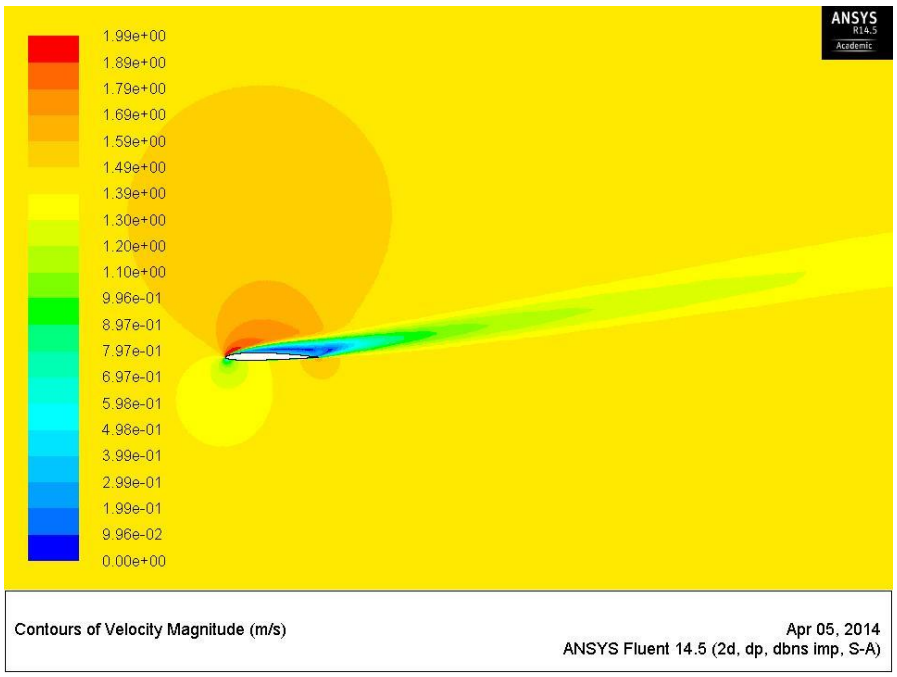

Looking at Figure 22, the overall velocity is higher than the previous case which is an anomaly. However the other differences make physical sense. Again the bottom of the tip and the top of the tail of the airfoil have slower velocities as they are stagnation and separation points. The top has a higher velocity due to the fact that the angle is causing more flow to go over the top of the airfoil than the bottom. This again confirms the reason why the pressure coefficient increased for the bottom of the airfoil.

8. COMPARISON OF FORM AND FRICTION ON DRAG

Table 6 shows the contribution of form drag and friction drag to the overall drag on the airfoil. As can be seen, the contribution of friction drag to the overall drag decreases as soon as the angle is changed from the reference angle ($\alpha = 0°$). In the case where all of the flow is in the x-direction, the flow should be relatively similar on the top and bottom of the airfoil which should cause minimal contribution form the pressure or form drag as shown in the case where $\alpha = 0°$. For the other cases where some of the velocity flows in the y-direction ($\alpha \neq 0°$), there is less air flowing parallel to the airfoil which causes less resistance from the airfoil and viscosity on the drag effect.

The form drag increases as the angle of attack changes because more of the flow is hitting the airflow perpendicularly and causing a pressure difference by forming around the airfoil. The total drag on the airfoil increases as the angle changes as the projected area on which the air hits increases known from the formula: $D = 1/2C_D A\rho V^2$.

Table 6: Contribution of Form and Friction to Drag

α	**Form Drag (N)**	**Friction Drag (N)**	**Total Drag (N)**	**Form (%)**	**Friction (%)**
-5	0.022708	0.012265	0.034973	64.93	35.07
0	0.006284	0.016621	0.022904	27.43	72.57
5	0.01648	0.014067	0.030547	53.95	46.05
10	0.140421	0.00531	0.14573	96.36	3.64

APPENDIX A

Table A-1: Coordinates of the NACA1408 Airfoil

#NACA1408				
#group	**#Point**	**#x_cord**	**#y_cord**	**#z_cord**
1	1	1	0.00084*	0
1	2	0.95016	0.00698	0
1	3	0.90027	0.01271	0
1	4	0.80039	0.02305	0
1	5	0.70041	0.03193	0
1	6	0.60034	0.03931	0
1	7	0.5002	0.04502	0
1	8	0.4	0.04869	0
1	9	0.2995	0.04939	0
1	10	0.24926	0.04819	0
1	11	0.19904	0.04574	0
1	12	0.14889	0.04171	0
1	13	0.09883	0.03558	0
1	14	0.07386	0.03138	0
1	15	0.04896	0.02602	0
1	16	0.02418	0.01862	0
1	17	0.01189	0.01324	0
1	18	0	0	0
1	19	0.01311	-0.012	0
1	20	0.02582	-0.0162	0
1	21	0.05104	-0.02134	0
1	22	0.07614	-0.02458	0
1	23	0.10117	-0.02682	0
1	24	0.15111	-0.02953	0
1	25	0.20096	-0.03074	0
1	26	0.25074	-0.03101	0
1	27	0.3005	-0.03063	0
1	28	0.4	-0.02869	0
1	29	0.4998	-0.02556	0
1	30	0.59966	-0.02153	0
1	31	0.69959	-0.01693	0
1	32	0.79961	-0.01193	0
1	33	0.89973	-0.00659	0
1	34	0.94984	-0.00378	0
1	0	1	-0.00084*	0

**Note: These values were changed to 0 in order to correct the mesh simulation.*